

Effects of Composition on Mechanical and Antibacterial Properties of Hydroxyapatite/Gray Titania Coating Fabricated by Suspension Plasma Spraying

Md Mirazul Mahmud Abir^a, Yuichi OTSUKA^b, Kiyoshi OHNUMA^c, Yukio MIYASHITA^d

^a Graduate School of Information and Control Engineering, Nagaoka University of Technology, 1603-1 Kamitomioka, Nagaoka-shi, Niigata 940-2188, Japan.

^b Department of System Safety, Nagaoka University of Technology, 1603-1 Kamitomioka, Nagaoka-shi, Niigata 940-2188, Japan.

^c Department of Biongingering, Department of Science of Technology Innovation, Nagaoka University of Technology, 1603-1 Kamitomioka, Nagaoka-shi, Niigata 940-2188, Japan.

^d Department of Mechanical Engineering, Nagaoka University of Technology, 1603-1 Kamitomioka, Nagaoka-shi, Niigata 940-2188, Japan.

Abstract

This study aims at revealing the effect of composition on mechanical and antibacterial properties of hydroxyapatite/gray Titania coating for biomedical applications. HAp is a bioceramic material used as a plasma-sprayed coating to promote osseointegration of femoral stems. Biomaterial coatings are fabricated mostly using atmospheric plasma spray (APS). However, the conventional plasma spray process requires hydroxyapatite powder with good flow, and to prepare such free-flowing powder, agglomeration, such as spray drying, fusing, and crushing is used. Therefore, it is impossible to spray nanopowder using conventional methods. Here, we designed a suspension-feeding system to feed nanoparticles using a liquid carrier. Suspension plasma spray (SPS) successfully deposited homogeneous HAp/Gray Titania coating with less porosity on the surface of titanium substrates. The microstructure of coatings with different compositions was then characterized using scanning electron microscopy, X-ray diffraction, and Raman spectroscopy to identify the crystal structure. All results consistently demonstrated that SPS could transform Ti_2O_3 into TiO_2 with mixed Magneli phases, such as Ti_4O_7 and Ti_3O_5 , which usually show photocatalytic activity. Inter-

Corresponding author: otsuka@vos.nagaokaut.ac.jp

facial strength, hardness, young modulus, and fracture toughness were also improved with a high concentration of TiO₂. Antibacterial test for *E. Coli* under LED light re-vealed that SPSed HAp/Gray Titania coating could significantly enhance antibacterial properties. The possible underlying mechanism of enhanced antibacterial properties can be attributed to increased Magneli phases and better bacterial adhesion caused by hydrophilic properties due to submicron size particles. SPS can fabricate visible light-responsive antibacterial coating, which can be used for medical devices.

Keywords: Hydroxyapatite, Gray Titania, Visible light sensitive photocatalyst, Suspension Plasma Spray, Interfacial strength, Antibacterial Property

1. Introduction

Aging people are suffering from locomotive diseases, such as osteoarthritis or associated symptoms in the bone tissue and joints [1]. Metallic implants to replace the deteriorated human bone have been widely used [2]. Commercially available pure titanium (cp-Ti ASTM F16) and titanium alloy Ti-6Al-4V ELI (extra-low interstitial) are the typical titanium alloys for biomedical applications. However, such the metallic biomaterials do not have any bioactivity to form a bond with surrounding tissues, which causes lower adhesive strength [1]. To overcome insufficient bonding, bioactive, as well as durable coating should be deposited onto the surface of metal implants [3].

Bioactive ceramics, which can promote osseointegration and osteoconduction, can form strong bonds and lead to enhanced durability of the implant when it is subjected to mechanical loading [3]. Hydroxyapatite [Ca₁₀(PO₄)₆(OH)₂, HAp], the most prominent bioactive ceramic which has a similar chemical composition to the human bone, has been widely used as an artificial bone or for coating metal implants to promote osteoconductivity [4]. However, HAp is a brittle ceramic material and then cannot be applied to a highly stressed area [5]. Development of HAp-based composite materials with TiO₂, Ytria Stabilized Zirconia, Alumina, Nanodiamond, Magnesium, or natural fiber, has been actively investigated to enhance mechanical properties of HAp [6, 7, 8, 9]. Mechanical properties of plasma-sprayed HAp coating was also reported and it is highly sensitive to crystallinity and the phase of HAp because its crystal struc-

ture changes to another phases of calcium phosphate during heating process [10]. Fatigue crack propagation of plasma-sprayed HAp coating is sensitive to cyclic loading and its microstructure should be considered to enhance its durability [3, 11, 12, 13] .

Another considerable function of the bioactive coating is antibacterial properties [14]. Infection of the implant due to bacterial adhesion is one of the main causes of implant failure [15]. Complications, such as tooth decay after long-term use or the need for joint replacement surgery, sometimes occur due to bacterial infection [14]. Several antibacterial coating methods have been proposed [16, 17], such the addition of the Ag ion [18], antibiotic peptide [19], and organic compounds [20]. A concept of multifunctional coating has recently been proposed [14], and coating with antibacterial properties, as well as high biocompatibility, is indispensable [21]. One possible multifunctional plasma-sprayed coating is a composite of HAp with a photocatalyst, such as TiO_2 , which provides a controllable release of radicals upon UV irradiation [22, 23, 24]. Unfortunately, UV irradiation is harmful to organs and visible light is more preferable. A composite plasma-sprayed coating of HAp with a visible light-responsive photocatalyst (TiO_2 -containing Magneli phases called "gray titania") has been successfully produced [25]. However, the composite HAp/Gray Titania coating has a relatively low bacterial adhesion and antibacterial properties, so the HAp complex [26, 27] was used to enhance cell adhesion, which demonstrated enhanced antibacterial property upon visible light irradiation [25, 21, 28]. The deficiency can be attributed to heating process during plasma spraying, which leads to low crystallinity of HAp thermal decomposition into more soluble phases (-TCP) [29, 30, 31]. Plasma spraying should be further considered to improve antibacterial properties of plasma-sprayed HAp composite coating.

Thermal spray technology, particularly atmospheric plasma spray (APS), is the accepted method by Food and Drug Administration (FDA, USA) to fabricate HAp coating for biomedical applications [32, 16, 17]. To suppress thermal decomposition, several spraying technologies have been developed, like vacuum plasma spray [33], cold spray [34], powder jet deposition [35], or aerosol deposition technology [36]. Vacuum thermal spray technology can reduce oxidation but the productivity is limited [33]. Cold spraying was also proposed to prevent particle melting during spraying. The

method was considered not applicable for ceramics [34]. Recently, jet deposition using fine particles in a vacuum was successfully applied to fabricate thin ceramics coatings [35, 36, 37]. However, the method is challenging when applying a thick coating in a short period. Suspension plasma spray (SPS) is an emerging coating technique that uses feedstock in the form suspension instead of dry powder, and therefore, it is capable of depositing nano-sized particles [38]. Poor flow of the ultrafine particle can be overcome by using a suspension flow system which can take particles to the center of the plasma jet [39, 40, 41]. Lower thermal decomposition is also expected due to the heat consumption effect by the solvent, which can lead to higher crystallinity of the HAp-based biomaterial coating [42]. However, the phase transformation of HAp and titania coating via SPS has not been studied and the effect of the composition on mechanical and antibacterial properties of SPS-HAp composite coating is not known.

This study aims at revealing the effect of composition on mechanical and antibacterial properties of HAp/Gray Titania coating for biomedical applications. Coating characterization was performed to investigate the microstructure and crystal structure. Scanning electron microscopy (SEM) was used to check the morphology of the coated specimen. Phase identification was performed using Horizontal X-ray diffraction (HAXRD) and Raman spectroscopy. Interfacial strength was determined by applying a tensile test using acoustic emission (AE) measurement system. Fracture toughness, hardness and young modulus of each type of coating were also evaluated to observe the effect of composition on mechanical properties. Finally, antibacterial properties of HAp/Gray Titania coating was evaluated by determining the number of colony forming units (CFU).

2. Experimental procedure

2.1. Preparation and characterization of powders

HAp powder (HAp-100 Taihei Chemical Industrial Co. Ltd., Japan) and titanium (III) Oxide (Ti_2O_3 , Wako Chemical Industry Co. Ltd., Japan) were used as feedstock powders to deposit suspension plasma-sprayed coatings. Both types of powders were ball milled for 72 h at 75 rpm using ceramic balls of 20-mm diameter and were subse-

quently sieved using # 45 m. The sieved particles were dispersed ultrasonically in the solution using a homogenizer for 20 min at a concentration of 30 wt.%. Distributions of particle size were measured using a laser diffraction particle size analyzer (LS-1300, Beckman Coulter, Inc., USA.). Morphologies of the powders were observed using a digital microscope (VHX-1000, Keyence CO. Ltd., Japan).

2.2. Preparation of the suspension

A mixture of water and ethanol at 1:1 ratio was selected, as shown in Table 1. Before adding the powder into the solvent it was measured to keep a concentration of 25 wt. %. The suspension was stirred for 3 h at 350 rpm using a mixer to disperse the particle in suspension. The suspension was then filtered through a sieve of 45 m mesh to further segregate the larger particles to avoid clogging during spraying. To improve the durability of the suspension, dispersing agent sodium hexametaphosphate at 0.8 wt. % was mixed with the suspension just before coating fabrication.

2.3. Material preparation and surface modification

Commercially pure titanium (cp-Ti) at a rectangular shape and Ti-6Al-4V ELI at a cylindrical bar shape were used for coating using SPS. The rectangular plates were used to determine the optimum condition for the suspension flow system, coating characterization, and the antibacterial test. The cylindrical specimens were used to determine the interfacial strength of the coating using tensile test under monotonic loading. The rectangular plates with at a size of 10 x 50x t3 mm³ were cut using a saw and, subsequently exposed to a milling machine and fine cutter to fit the specimen properly into the jig. The round bar specimen at a length of 60 mm and a diameter of 15 mm was prepared using a lathe machine and fine cutter. After completing all these processes, the surface of all specimens was mechanically ground using a grinding machine. The specimens were then ultrasonically cleaned with ethanol for 15 min and dried in a hot air drier. Before SPS, the surface of the substrate was polished using emery paper of # 80 to #1000 and treated with grit blasting using alumina particle 30, at a spraying pressure of 5 MPa. Once the surface of the specimen was blasted to create the desired roughness, they were cleaned ultrasonically using ethanol for 20 min.

2.4. Fabrication of Coating by SPS

A suspension flow system was designed and assembled with a plasma gun system. Four different compositions of the feedstock were used to evaluate the effects of composition on mechanical and antibacterial properties of the SPS-HAp composite coating. The coated layer was deposited using a commercial plasma spray machine (Model 9MB, Sulzer-Metco Ltd) connected to a suspension flow system at an optimized operating condition, as shown in Table 1. The desired thickness of the suspension plasma-sprayed coating layer was 100-150 μm .

2.5. Coating characterization

After fabrication of the coating, the morphology of the specimen was investigated using SEM (JEOL-JCM 6000 Plus, NeoScope, JEOL, Japan). Image of the surface microstructure was captured by detecting the secondary electron (High-vac) upon exciting the atoms using an electron beam at a voltage of 5 kV. The crystalline phases of the coating were identified using HXRD (Smart Lab 9KW, Rigaku, CO. Ltd. Japan) at CuK radiation, a grazing incident of 2° , a voltage of 45 kV and a current of 200 mA. HAp (ICDD 00-009-0432), rutile (ICDD 00-001-1292), anatase (ICDD 00-001-0562), Ti_6O_{11} (ICDD 01-076-1266), Ti_5O_9 (ICDD 01-071-0627), Ti_4O_7 (ICDD 01-077-1390), and Ti_3O_5 (00-023-0606) were used in the Rietveld analysis. XRD data of pure titanium has also taken to remove the peak coming from the substrate.

Raman spectroscopy (Lab-RAM HR-800, Horiba Jobin YVON) was conducted to identify the phase distribution of the coatings. The conditions were as follows: Laser wavelength of 532 nm; laser power of 50 mW; slit size of 100 μm ; hole size of 500 μm ; objective lens magnification of x100; observation area of (100 x 100) μm^2 ; exposure time of 3 s; accumulation number of 5. Raman spectroscopy of unheated HAp, Ti_2O_3 , HAp/titania, rutile, and anatase were also investigated as reference data. In addition, phase analysis of the coating was performed via XRD Rietveld and Raman peak fitting analysis using Gaussian equation. The contact angle was also measured using 1 μL droplets.

2.6. Interfacial strength test

Interfacial test following ASTM F1147-05 & JSME standard S019 was conducted using the autograph (AGS-X 10N-10KN Shimadzu co. Ltd. Japan) with a cross-head displacement rate of 1 mm/min. Adhesion of the specimen using the metal lock Y610 was performed following the method proposed by Otsuka et al.[43]. A strain gauge was attached at the bottom of the specimen 10 mm from the coating layer. To detect the failure of the coated layer, AE system with fast Fourier analysis (FFT) were used with a total gain of 80 dB and V_L & V_H were respectively 0.4 and 1 V. Interfacial strength was calculated by dividing the maximum load by the nominal area.

Fracture surfaces (both the adhesive side and the coating side) were observed using a digital microscope and images of the fracture surface were obtained. Raman spectroscopy was conducted on the coated side to confirm the absence of infiltrations of the adhesive into HAp/Gray Titania coating during the tensile test. Infiltration was prohibited to obtain valid values for the bonding strength of the coating.

2.7. Hardness and Young modulus test

Hardness and young modulus were determined using dynamic microhardness test-ing machine (DUH-211S, Shimadzu, Japan). Testing was conducted on polished cross-sectional surfaces of the embedded specimen under a load of 200 mN. Time set for both loading and unloading was 15 s and holding time was 5 s. A total of ten points were selected for each type of coating to obtain the hardness and young modulus values. Mean and standard deviation of data from ten points was subsequently calculated.

2.8. Fracture toughness test

Fracture toughness was evaluated using the indentation fracture (IF) method with a dynamic microhardness testing machine (DUH-211S, Shimadzu, Japan). To evaluate K_{IC} using the IF method, several equations were proposed, some of which required of young and Poisson modulus values in addition to hardness values. Niihara's equation,

1, was used to calculate the fracture toughness value.

$$K_{IC} = 0.067(E=Hv)^{0.4}(Hv)(\alpha)^{0.5}(c=a)^{1.5} \quad (1)$$

K_{IC} : Fracture Toughness (MPa $m^{1/2}$)

H : Vickers Hardness [MPa]

P : Test Load in Vickers Hardness Test [MPa]

E : Young Modulus [MPa]

a : Half average length of the diagonal of Vickers marks[m]

c : Average length of the crack obtained in the tip of the Vickers hardness marks[m]

2.9. Antibacterial test

The antibacterial test was conducted using E. coli (K-12 strain, NBRC 3301, National Institute of Technology and Evaluation, Japan) to investigate the effect of the composition of SPS-HAp/Gray Titania coating on antibacterial properties. CFU values were counted to estimate the number of viable bacteria in a sample. Three types of visible light, blue, green, and red, were used to irradiate the samples for 1 h, keeping the intensity value of 50 mW/cm m^2 . The wavelength of the three types of visible light was measured using a spectrometer (MK 350N premium) before the test. The Luria Bertani (LB) medium consisted of Bacto tryptone (10 g/L), Bacto yeast extract (5 g/L), NaCl (10 g/L), and deionized water. Agar medium consisted of Bacto tryptone (10 g/L), Bacto yeast extract (5 g/L), NaCl (10 g/L), Bacto Agar (15g/L), and deion-ized water. Both media were then sterilized in an autoclave at 120 o C and 15 psi for 2 h. (TOMY, SX-500) The initial concentration of the of E. coli suspension was 10 5 CFU/ml. Droplets of E. Coli suspension (100 l) placed on the surface of the coating (10 x 10 mm) following the international standard for antibacterial tests. Visible light was irradiated from the top of the coating for 1 h. The E. coli suspension, following the light irradiation, was diluted 10 4 times. After that, 0.1 mL of the diluted suspension was grown on agar medium and incubated at 37 o C for 18 h, as shown in Figure 1. Finally, Colonies on the nutrient agar medium were counted using AI camera. CFU was calculated.

Cell viability was evaluated to reveal the intensity of the live/dead cells on the surface of each coating after light irradiation. *E. coli* nuclei were stained using SYTO 9 from Thermo Fisher Scientific Inc. following the manufacturer's instructions. Then, adhesion and viability of *E. coli* were visualized using a fluorescence microscope (BZ-8100, Keyence Co. Ltd.).

ANOVA and several comparison by Holm's method were applied to the result of the antibacterial test. The significance level was set to $p < 0.05$. All statistical analyses were performed using the R4.0.3 software.

3. Results

3.1. Characterization of feedstocks

Figure 2 (a & b) shows the typical surface morphology of the submicron-sized powders. The microscopic image depicts the homogeneous distribution of the particle with little agglomeration. Moreover, the agglomerated powders could be dispersed easily in the suspension. Figure 2 (c) shows particle size distribution of HAp and Ti₂O₃ powder. The mean size of HAp was 0.775 μ m and that of Ti₂O₃ was 0.535 μ m. This result certified that powder size was much smaller than the ones used for a conventional APS technology, which were more than 45 μ m. Larger variation in the sizes of Ti₂O₃ powders were probably due to hardness, which would resist to fractures during the ball milling process.

3.2. Coating features deposited by SPS

Figure 3 shows the surface morphologies of for all four types of coating deposited using SPS. The suspension plasma-sprayed coating exhibited white color for pure HAp coating and became more black with the increasing concentration of Ti₂O₃. Only in the case of HAp 50:Ti₂O₃ 50 showed gray color, which might be associated with higher heat consumption during the coating deposition process. Figure 4 (a-d) shows the surface microstructure of HAp/Gray Titania coatings deposited by SPS at optimized conditions. The surface of the HAp/Gray Titania coating showed homogeneous features with low porosity. Figure 4 (e-h) depicts the highly magnified SEM images of the coatings. Splats were flattened and few spherical splats were observed, which suggested

that particles were sufficiently melted during SPS [44]. The splats were well connected, which was expected to provide high cohesion strength of the coatings. Porosity distribution and thickness of each type of coating are summarized in table 2. The thickness of the coating layers was 70-100 μm , which was compatible with the ones fabricated using the conventional APS method. Porosity of the coatings decreased with the increasing concentration of Ti_2O_3 in the suspension.

3.3. Phase identification of the coating

The microstructure of HAp/Titania coating was also characterized using Raman spectroscopy and HXRD to identify the crystal structure and phase distribution of the coating. Figure 5 (a-d) shows the XRD patterns of the coating deposited by SPS. Though the primal peak at approximately $2\theta = 32.0^\circ$ had a shoulder due to formation of β -TCP, the main phase showed HAp with higher crystallinity [45]. For four types of composite coating, Ti_2O_3 was thermally oxidized into anatase or rutile (TiO_2). SPS could decompose Ti_2O_3 into mixed Magneli phases of TiO_2 , Ti_4O_7 and Ti_3O_5 phases were detected, which usually shows photocatalytic activity by visible light irradiation [46]. Matsuya et. al. observed the different phase Ti_6O_{11} in their composite coating fabricated by APS [25]. SPS produced the Titania coating with Magneli phases effectively, which enhanced antibacterial properties.

Figure 6 (a-d) shows the Raman spectroscopy results of coatings. Pure HAp coating had the main peak from 961 cm^{-1} , which was due to the ν_1 stretch of PO_4^{3-} in the HAp crystal. Besides the peak from HAp, we also observed peaks from rutile and anatase phases of TiO_2 , which were compatible the ones observed using unheated rutile and anatase TiO_2 powders. Raman spectroscopy results also indicated the existence of Magneli phases by showing a strong peak of Ti_4O_7 and Ti_3O_5 . The vibrational frequencies at 240, 247, and 605 cm^{-1} were from Ti_4O_7 and the frequency at 265, 615 cm^{-1} were from Ti_3O_5 . Consequently, SPS produced composite coating, containing oxygen-deficient types of titania, which could be used as a visible light responsive photocatalyst. In this study, Gaussian fitting was used to study the detailed bonding structure of titanium and oxygen. Peak distribution from $500\text{ to }800\text{ cm}^{-1}$ was fitted to analyze the available phases. However, the peak produced by PO_4^{3-} due to the HAp

crystal was the obstacle for detecting the peak solely obtained from the phases of TiO_2 . Hence, the substitution of the peak from HAp (both primary and secondary peaks) was performed to avoid all the peaks from the HAp coating.

Volumetric composition of Magneli phases for all three types of coating was also evaluated using both Raman multiple peak fitting analysis and XRD Rietveld quantitative analysis (Figure 7). Both Raman and XRD results consistently exhibited that Magneli phases were increased with the increasing nominal composition of Ti_2O_3 .

3.4. Interfacial strength via tensile testing

Figure 8 (a) shows the stress-strain curve during interfacial strength tests. The stress-strain curve showed a linear line. AE signals were detected only in the final stage close to fracture. The number of detected AE signals were reduced compared to the case of HAp coating deposited by APS, which was due to reduced porosity. Interfacial strength of HAp coating was approximately 15 MPa, which was higher than that of HAp coating by APS (approximately 10 MPa) [43] and the strength for composite coating was slightly increased with the increasing Ti_2O_3 concentration (Figure 8 (d)). There was a little time lag in detecting two AE signals during the tests, which suggested that the damage occurred at the midpoint of two sensors; in the coating or adhesive layer of both HAp and composite coatings (Figure 8 (b)). FFT analyses showed that the main frequency domain was approximately 500 kHz for both HAp and composite coatings (Figure 8 (c)). Such AE signals were usually observed in the cracking of HAp coating, which suggested the validity of interfacial tests [47]. Infiltration of adhesive was abstained, which certified that the strength detected using the tensile test was the interfacial strength of the coating with substrate.

3.5. Hardness and Young modulus test

Figure 9 (a) and figure 9 (b) show the effect of Ti_2O_3 addition in suspension on mechanical properties of HAp/ Titania composite coating. Both values were significantly increased with the increasing concentration of Ti_2O_3 in the suspension due to homogeneous dispersion of harder TiO_2 particles in the coatings.

3.6. Fracture toughness test

The result of the fracture toughness test using IF method is depicted in figure 9 (c). Pure HAp coating exhibited a fracture toughness of $1.14 \text{ MPam}^{1/2}$. Addition of Ti_2O_3 enhanced the fracture toughness probably due to reduced porosity and fewer number of microcracks presented in the composite coating.

3.7. Antibacterial activity of HAp/gray Titania coating

Results of the wavelength for three types of light is shown in figure 10. It was observed that wavelengths of the blue, green, and red lights were 447, 518, and 635 nm respectively. CFU for various compositions of HAp/Gray Titania coating was evaluated as depicted in figure 11. CFU of the SPS 80H20T sample was approximately 20 % lower than that of the pure HAp sample. There was no reduction in CFU with no sample, which suggested that the enhanced antibacterial property was not attributed to heating by irradiation but to photocatalytic effects of the SPS-HAp/Gray Titania coating. The reduction effects on CFUs by titania containing groups (80H20T, 60H40T, and 50H50T) and laser irradiation were significant ($F(4) = 72.95, p < 0.001, F(3) = 16.4, p < 0.001$), whereas an interaction effect (*group*) (*laser*) was weakly significant ($F(12) = 1.85, p = 0.072$). Detailed analyses by multiple regression analyses revealed that the interaction effects of titania containing groups (60H40T and 50H50T) with light irradiation (Blue, Green, and Red) were significant ($t = 2.98, p = 0.005$ (50H50T Red irradiation)). These results certified that the new SPS composite coating could successfully improve the antibacterial properties. CFU was further decreased by increasing the weight percentage of the antibacterial agent (Gray titania: TiO_2 containing magneli phases).

The antibacterial efficiency of the SPS composite coating was also assessed via the live/dead bacterial viability assay. As red light irradiation showed remarkable reduction in CFU, we checked cell viability only in the presence of red light irradiation for all four types of coating. As shown in figure 12 (b-e), the number of live bacteria (green) on pure HAp coating was more than that on other composite coatings, and almost no dead cells (red) were found. The intensity of the live/dead cell ratio for all four types of coating was calculated as shown in figure 12 (a). This result also confirmed that the

bacterial growth was inhibited on the surface of the composite coating. Consequently, the addition of TiO_2 enhanced the antibacterial property of the SPS composite coating under visible light irradiation, and 50H50T coating showed the maximum efficiency in this regard.

3.8. Contact angle of coating

The contact angle was measured for all four types of coating, and pure titanium. Figure 13 shows that HAp coating exhibited hydrophilic behavior, whereas the composite coating was not hydrophobic. Meaning that SPS composite coating resulted in hydrophilic surfaces. However, wettability was decreased with higher concentration of TiO_2 .

4. Discussion

This study aimed at observing the effects of composition on mechanical, and antibacterial properties of HAp/ Gray Titania coating fabricated by SPS. New suspension-feeding system was successfully attached to the conventional APS gun, which enabled us to directly compare the mechanical properties of plasma-sprayed coating fabricated using different feeding methods, air or suspension. SPS could produce a homogeneous composite coating with lower porosity, which enhanced hardness, young's modulus, and fracture toughness by increasing the concentration of Ti_2O_3 in the suspension (Figure 4, Figure 8). Interfacial strength of the composite coating was slightly increased with the increasing concentration of Ti_2O_3 in the suspension. (Figure 9). SPS specifically suppressed the oxidation of Ti_2O_3 , and the resultant composition of the coatings successfully contained Magneli phases of titania (Figure 5, Figure 6, Figure 7), which could enhance photocatalytic property of the composite coating under irradiation with visible light (Figure 11, Figure 12). Probable enhancement mechanisms in mechanical and antibacterial properties of SPS-HAp/Gray Titania coating are discussed below.

4.1. Enhancement of mechanical properties of the SPS-HAp composite coating

Tensile test results demonstrated that the strength of the HAp coating was approximately 15 MPa, which was significantly higher than that of the HAp coating deposited using conventional APS method [43]. The higher strength of the SPS-HAp coating might be attributed to lower particle size, lower porosity, and higher crystallinity. Fine particles were partially melted, which improved the bonding strength among splats and reduced porosity. TiO_2 dispersing was possibly due to unchanged bonding conditions between both layers. The reinforcement of Ti_2O_3 in HAp significantly enhanced the hardness, young modulus and fracture toughness of the coating. The cohesive strength of HAp coating was significantly improved by dispersing TiO_2 . Higher crystallinity of the HAp coating, which was attributed to evaporation of the solvent during SPS, could increase cohesive strength of the coating layer because of suppressed formation of the amorphous interface layer. Therefore, the HAp coating deposited by the novel SPS method showed higher interfacial strength than APS coating.

4.2. Enhancement mechanism of antibacterial properties of the SPSed HAp composite coating

In conventional APS process, HAp particles were impacted on the substrate and then cooled down, which led to the formation of thermally decomposed phases or amorphous phases, such as tri calcium phosphate, tetra calcium phosphate, and CaO, which reduced crystallinity of the coating layer. [48]. Such lower crystallinity and low coating strength were not beneficial for the mechanical integrity *in vivo*. In contrast, during SPS process, the temperature gap between molten material and the substrate was lower due to heat consumption by the solvent. Such exploitation of heat by evaporation of the solvent helped reduce the cooling rate of the particle and subsequently reduced the formation of the amorphous phase, which led to higher crystallinity of HAp coating [49]. In addition, composite coating contained several Magneli phases, such as Ti_4O_7 / Ti_3O_5 , which showed stronger photocatalytic activity than other Magneli phases detected in previous studies [25]. Our present study revealed that SPS could provide TiO_2 coating with Magneli phases. The band gap energy of Magneli phases is

approximately 0.5 eV narrower than that of anatase TiO₂ (3.2 eV) [50]. Morakul et. al. have demonstrated that the composite coating of HAp with titania exhibits antibacterial properties against *E. Coli* under visible light irradiation, such as blue(450nm=2.76eV), green(532nm=2.33 eV), and red (633nm=1.96eV) [21]. Formation of such Magneli phases could contribute the enhanced antibacterial properties using visible light.

Enhancement mechanism using fine particles in HAp composite coating is illustrated in figure 14. In the case of SPS composite coating, the grain size was around 2 μ m, which could only accommodate 1 or 2 *E. coli* bacteria, which increased the contact distance between coating particle and bacteria, so that the bacteria was more exposed to released reactive oxygen species (ROS). On the contrary, for conventional composite coating, the grain size was quite big (10 μ m), and the number of adhered bacteria on each grain was more than that obtained using SPS coating. It is not practically possible for each radical to go through a large number of bacteria. As a result, many bacteria did not come in contact with ROS and remained alive. Contact angle of the SPS-HAp coating was superhydrophilic, which also played a supportive role to enhance bacterial adhesion onto coating surfaces. Consequently, the particle size in the coating was a considerable factor in enhancing the antibacterial property of HAp composite coating.

In this study, SPS could successfully modify the microstructure and crystallographic structure of the coating material by utilizing the nanoparticle in the form of suspension, which was favorable for antibacterial properties. The solid concentration (weight percentage of the particle) and solvent (both aqueous and alcoholic) played an important role on the microstructure of the coating. Optimizing such parameters of SPS led to the control of the coating microstructure. On the contrary, cortical bone on the surface provides higher mechanical strength due to their complex dense structure, and cancellous bone inside enables blood circulation and bone ingrowth attributing to their porous structure[51]. Both composition and porosity gradient layers should be combined in single coating structure in order to mimic the structure of human bone. Outer layer should be porous, made up of HAp, whereas the inner layer should be compact containing the metal. The present study does not fulfill the requirement of the ideal coating to be applied in implants. Therefore, it is further important to challenge functionally graded coating for biomedical application[52].

5. Conclusion

This study investigated the effects of composition on mechanical and antibacterial properties of hydroxyapatite /gray titania coating fabricated by suspension plasma spray. The main conclusions obtained are as follows:

1. SPS successfully deposited composite coating of HAp with Ti_2O_3 of different compositions onto the surface of the titanium substrate. The microstructure of the coating certified that particle distribution was homogeneous, most of the splats were flattened and melted properly, which resulted in low porosity.
2. HAp coating showed very high crystallinity and composite coating contained mainly rutile and anatase phases. SPS also provided TiO_2 coating with oxygen-deficient types of titanium oxides. *e.g.*, Magneli phase, which can be activated by visible light irradiation.
3. The enhanced antibacterial property of the SPS-HAp/Gray Titania coating can be attributed to high composition of Magneli phases and high wettability.

This study revealed that finer particles in the microstructure of the HAp/ Gray Titania promote visible light sensitivity, which provides superior antibacterial properties. Optimization of process parameters and coating layers should be further considered in future studies.

Acknowledgments

We thank Niigata Metalicon Co., Ltd., for producing the plasma-sprayed samples. We also thank the analytical center of Nagaoka University of Technology for their supports in XRD and SEM observations. This study was partially supported by JSPS KAKENHI 17H04898 ,Union Tool Foundations and TAKEUCHI foundations.

References

- [1] W. Harun, R. Asri, J. Alias, F. Zulkifli, K. Kadirgama, S. Ghani, J. Sharifuddin, A comprehensive review of hydroxyapatite-based coatings adhesion on metallic biomaterials, *Ceramics International* 44 (2) (2018) 1250 – 1268.

doi:<https://doi.org/10.1016/j.ceramint.2017.10.162>.

URL <http://www.sciencedirect.com/science/article/pii/S0272884217323635>

- [2] Q. Chen, G. A. Thouas, Metallic implant biomaterials, *Materials Science and Engineering: R: Reports* 87 (2015) 1 – 57. doi:<https://doi.org/10.1016/j.mser.2014.10.001>.

URL <http://www.sciencedirect.com/science/article/pii/S0927796X14001077>

- [3] Y. Otsuka, D. Kojima, Y. Mutoh, Prediction of cyclic delamination lives of plasma-sprayed hydroxyapatite coating on ti-6al-4v substrates with considering wear and dissolutions, *Journal of the Mechanical Behavior of Biomedical Materials* 64 (2016) 113 – 124. doi:<http://dx.doi.org/10.1016/j.jmbbm.2016.07.026>.

URL <http://www.sciencedirect.com/science/article/pii/S1751616116302429>

- [4] H. Xu, X. Geng, G. Liu, J. Xiao, D. Li, Y. Zhang, P. Zhu, C. Zhang, Deposition, nanostructure and phase composition of suspension plasma-sprayed hydroxyapatite coatings, *Ceramics International* 42 (7) (2016) 8684 – 8690. doi:<https://doi.org/10.1016/j.ceramint.2016.02.102>.

URL <http://www.sciencedirect.com/science/article/pii/S027288421630044X>

- [5] V. Sergo, O. Sbaizero, D. R. Clarke, Mechanical and chemical consequences of the residual stresses in plasma sprayed hydroxyapatite coatings, *Biomaterials* 18 (6) (1997) 477 – 482. doi:[https://doi.org/10.1016/S0142-9612\(96\)00147-0](https://doi.org/10.1016/S0142-9612(96)00147-0).

URL <http://www.sciencedirect.com/science/article/pii/S0142961296001470>

- [6] X. Chen, B. Zhang, Y. Gong, P. Zhou, H. Li, Mechanical properties of nanodiamond-reinforced hydroxyapatite composite coatings deposited by

suspension plasma spraying, *Applied Surface Science* 439 (2018) 60 – 65.
doi:<https://doi.org/10.1016/j.apsusc.2018.01.014>.
URL <http://www.sciencedirect.com/science/article/pii/S0169433218300163>

[7] A. A. Vu, S. F. Robertson, D. Ke, A. Bandyopadhyay, S. Bose, Mechanical and biological properties of zno, sio₂, and ag₂o doped plasma sprayed hydroxyapatite coating for orthopaedic and dental applications, *Acta Biomaterialia* 92 (2019) 325 – 335. doi:<https://doi.org/10.1016/j.actbio.2019.05.020>.
URL <http://www.sciencedirect.com/science/article/pii/S174270611930337X>

[8] M. F. Vassal, J. Nunes-Pereira, S. P. Miguel, I. J. Correia, A. P. Silva, Microstructural, mechanical and biological properties of hydroxyapatite - cazro₃ biocomposites, *Ceramics International* 45 (7, Part A) (2019) 8195 – 8203. doi:<https://doi.org/10.1016/j.ceramint.2019.01.122>.
URL <http://www.sciencedirect.com/science/article/pii/S0272884219301270>

[9] D. Khazeni, M. Saremi, R. Soltani, Development of ha-cnts composite coating on az31 magnesium alloy by cathodic electrodeposition. part 1: Microstructural and mechanical characterization, *Ceramics International* 45 (9) (2019) 11174 – 11185. doi:<https://doi.org/10.1016/j.ceramint.2019.02.143>.
URL <http://www.sciencedirect.com/science/article/pii/S0272884219304456>

[10] S. Yugeswaran, C. Yoganand, A. Kobayashi, K. Paraskevopoulos, B. Subramanian, Mechanical properties, electrochemical corrosion and in-vitro bioactivity of yttria stabilized zirconia reinforced hydroxyapatite coatings prepared by gas tunnel type plasma spraying, *Journal of the Mechanical Behavior of Biomedical Materials* 9 (2012) 22 – 33. doi:<https://doi.org/10.1016/j.jmbbm.2011.11.002>.

URL <http://www.sciencedirect.com/science/article/pii/S1751616111002852>

- [11] A. R. Nimkerdphol, Y. Otsuka, Y. Mutoh, Effect of dissolution/precipitation on the residual stress redistribution of plasma-sprayed hydroxyapatite coating on titanium substrate in simulated body fluid (sbf), *Journal of the Mechanical Behavior of Biomedical Materials* 36 (0) (2014) 98 – 108.
- [12] Y. OTSUKA, Y. MIYASHITA, Y. MUTOH, Effects of delamination on fretting wear behaviors of plasma-sprayed hydroxyapatite coating, *Mechanical Engineering Journal* 3 (2) (2016) 15–00573–15–00573. doi:10.1299/mej.15-00573.
- [13] Y. Otsuka, H. Kawaguchi, Y. Mutoh, Cyclic delamination behavior of plasma-sprayed hydroxyapatite coating on ti–6al–4v substrates in simulated body fluid, *Materials Science and Engineering: C* 67 (2016) 533 – 541. doi:<http://dx.doi.org/10.1016/j.msec.2016.05.058>.
URL <http://www.sciencedirect.com/science/article/pii/S092849311630491X>
- [14] J. Raphel, M. Holodniy, S. Goodman, S. Heilshorn, Multifunctional coatings to simultaneously promote osseointegration and prevent infection of orthopaedic implants, *Biomaterials* 84 (2016) 301–314, cited By 306. doi:10.1016/j.biomaterials.2016.01.016.
URL <https://www.scopus.com/inward/record.uri?eid=2-s2.0-84992447299&doi=10.1016%2fj.biomaterials.2016.01.016&partnerID=40&md5=0e68ec6bd13546f64f3369eebc432cee>
- [15] Z. Khatoon, C. D. McTiernan, E. J. Suuronen, T.-F. Mah, E. I. Alarcon, Bacterial biofilm formation on implantable devices and approaches to its treatment and prevention, *Heliyon* 4 (12) (2018) e01067. doi:<https://doi.org/10.1016/j.heliyon.2018.e01067>.
URL <http://www.sciencedirect.com/science/article/pii/S2405844018369019>

- [16] R. Heiman, H. Lehmann, Bioceramic coatings for medical implants, Wiley-VCH Weinheim.
- [17] R. Surmenev, M.a. surmeneva, and a.a. ivanova, significance of calcium phosphate coatings for the enhancement of new bone osteogenesis—a review, *Acta Biomater* 10 (2014) p 557–570.
- [18] W. Chen, Y. Liu, H. Courtney, M. Bettenga, C. Agrawal, J. Bumgardner, J. Ong, In vitro anti-bacterial and biological properties of magnetron co-sputtered silver-containing hydroxyapatite coating, *Biomaterials* 27 (32) (2006) 5512 – 5517. doi:<https://doi.org/10.1016/j.biomaterials.2006.07.003>.
URL <http://www.sciencedirect.com/science/article/pii/S014296120600593X>
- [19] M. Kazemzadeh-Narbat, B. F. Lai, C. Ding, J. N. Kizhakkedathu, R. E. Hancock, R. Wang, Multilayered coating on titanium for controlled re-lease of antimicrobial peptides for the prevention of implant-associated infections, *Biomaterials* 34 (24) (2013) 5969 – 5977. doi:<https://doi.org/10.1016/j.biomaterials.2013.04.036>.
URL <http://www.sciencedirect.com/science/article/pii/S0142961213004808>
- [20] J. Shen, B. Jin, Y. cheng Qi, Q. ying Jiang, X. feng Gao, Carboxylated chitosan/silver-hydroxyapatite hybrid microspheres with improved antibacterial activity and cytocompatibility, *Materials Science and Engineering: C* 78 (2017) 589 – 597. doi:<https://doi.org/10.1016/j.msec.2017.03.100>.
URL <http://www.sciencedirect.com/science/article/pii/S0928493116314345>
- [21] S. Morakul, Y. Otsuka, K. Ohnuma, M. Tagaya, S. Motozuka, Y. Miyashita, Y. Mutoh, Enhancement effect on antibacterial property of gray titania coating by plasma-sprayed hydroxyapatite-amino acid complexes during irradiation with visible light, *Heliyon* 5 (8) (2019) e02207. doi:<https://doi.org/10.1016/j.heliyon.2019.e02207>.

URL <http://www.sciencedirect.com/science/article/pii/S2405844019358670>

- [22] J. U., Juganson, K., Visnapuu, M., Mortimer, M., Kahru, A., Nommiste, E., Joost, U., Kisand, V., I. A., Photocatalytic antibacterial activity of nano-tio₂ (anatase)-based thin films: Effects on escherichia coli cells and fatty acids, *Journal of Photochemistry and Photobiology B: Biology* 142 (2015) 178–185, cited By :104.

URL www.scopus.com

- [23] X. Zheng, C. Ding, Characterization of plasma-sprayed hydroxyapatite/tio₂ composite coatings, *Journal of thermal spray technology* 9 (4) (2000) 520–525.

- [24] A. Nakajima, K. Takakuwa, Y. Kameshima, M. Hagiwara, S. Sato, Y. Yamamoto, N. Yoshida, T. Watanabe, K. Okada, Preparation and properties of titania–apatite hybrid films, *Journal of Photochemistry and Photobiology A: Chemistry* 177 (1) (2006) 94 – 99. doi:<https://doi.org/10.1016/j.jphotochem.2005.05.019>.

URL <http://www.sciencedirect.com/science/article/pii/S1010603005002790>

- [25] T. Matsuya, S. Morakul, Y. Otsuka, K. Ohnuma, M. Tagaya, S. Motozuka, Y. Miyashita, Y. Mutoh, Visible light-induced antibacterial effects of the luminescent complex of hydroxyapatite and 8-hydroxyquinoline with gray titania coating, *Applied Surface Science* 448 (2018) 529 – 538. doi:<https://doi.org/10.1016/j.apsusc.2018.04.106>.

URL <http://www.sciencedirect.com/science/article/pii/S0169433218310687>

- [26] T. Matsuya, Y. Otsuka, M. Tagaya, S. Motozuka, K. Ohnuma, Y. Mutoh, Formation of stacked luminescent complex of 8-hydroxyquinoline molecules on hydroxyapatite coating by using cold isostatic pressing, *Materials Science and Engineering C* 58 (2016) 127–132.

URL <http://www.sciencedirect.com/science/article/pii/S0928493115302757>

- [27] S. Morakul, Y. Otsuka, A. Nararya, M. Tagaya, S. Motozuka, K. Ohnuma, Y. Miyashita, Y. Mutoh, Effects of compression on orientation of ligands in fluorescent complexes between hydroxyapatite with amino acids and their optical properties, *Journal of the Mechanical Behavior of Biomedical Materials* 88 (2018) 406 – 414. doi:<https://doi.org/10.1016/j.jmbbm.2018.09.006>.
URL <http://www.sciencedirect.com/science/article/pii/S1751616118309160>

- [28] K. Leelanarathiwat, Y. Katsuta, Y. Otsuka, H. Katsuragi, F. Watanabe, The antibacterial activity of hydroxyapatite-tryptophan complex with gray titania by photocatalysis using led diodes., *International Journal of Oral & Maxillofacial Implants* 35 (2) (2020) 265–274. doi:0.11607/jomi.7742.

- [29] J. Heughebaert, G. Montel, Conversion of amorphous tricalcium phosphate into apatitic tricalcium phosphate, *Calcif. Tissue Int.* 34 (1982) p S103–S108.

- [30] R. B. Heimann, Thermal spraying of biomaterials, *Surface and Coatings Technology* 201 (5) (2006) 2012 – 2019, the 2nd International Meeting on Thermal Spraying. doi:<https://doi.org/10.1016/j.surfcoat.2006.04.052>.
URL <http://www.sciencedirect.com/science/article/pii/S0257897206003951>

- [31] B. Leon, J. Jansen, *Thin calcium phosphate coatings for medical implants*, Springer.

- [32] FDA, Guidance for industry and fda staff—class ii special controls guidance document: Root-form endosseous dental implants and endosseous dental abutments. u.s, Dept. of Health and Human Services, Silver Spring, MD.

- [33] H. Gruner, Coating of an implant body, *Intern. Pat. Appl.* WO 1 A1 (986/006617).

- [34] J. Tang, Z. Zhao, H. Liu, X. Cui, J. Wang, T. Xiong, A novel bioactive ta/hydroxyapatite composite coating fabricated by cold spraying, *Materials Letters* 250 (2019) 197 – 201. doi:<https://doi.org/10.1016/j.matlet.2019.04.123>.

URL <http://www.sciencedirect.com/science/article/pii/S0167577X19306937>

- [35] N. YOSHIHARA, T. KURIYAGAWA, Y. YASUTOMI, K. OGAWA, Powder jet deposition of ceramic films (materials processes and micro-manufacturing for science), Proceedings of International Conference on Leading Edge Manufacturing in 21st century : LEM21 2005.2 (2005) 833–838. doi:10.1299/jsmelem.2005.2. 833.
- [36] J. Akedo, Room temperature impact consolidation (rtic) of fine ceramic powder by aerosol deposition method and applications to microdevices, Journal of Thermal Spray Technology 17 (2008) 181–198. doi:<https://doi.org/10.1007/s11666-008-9163-7>.
- [37] S. R.B. Heimann, Properties, and biomedical performance of osteoconductive bioceramic coatings, Surf. Coat. Technol. 233 (2013) p 27–38.
- [38] L. Pawlowski, Suspension and solution thermal spray coatings, Surface and Coatings Technology 203 (19) (2009) 2807 – 2829. doi:<https://doi.org/10.1016/j.surfcoat.2009.03.005>.
URL <http://www.sciencedirect.com/science/article/pii/S025789720900228X>
- [39] M. Vicent, E. Bannier, P. Carpio, E. Rayon, R. Benavente, M. Salvador, E. Sanchez, Effect of the initial particle size distribution on the properties of suspension plasma sprayed al₂o₃–tio₂ coatings, Surface and Coatings Technology 268 (2015) 209 – 215, 6th Rencontres Internationales de la Projection Thermique. doi:<https://doi.org/10.1016/j.surfcoat.2014.12.010>.
URL <http://www.sciencedirect.com/science/article/pii/S0257897214011426>
- [40] J.-E. Otterstedt, D. A. Brandreth, Small particles technology, Springer Science & Business Media, 2013.

- [41] C. L. F L Toma, A Potthoff, Demands, potential, and economic aspects of thermal spraying with suspensions: a critical review, *J. Therm. Spray. Technol.* 24 (7) (2015) pp. 1143–1152.
- [42] B. Zheng, Y. Luo, H. Liao, C. Zhang, Investigation of the crystallinity of suspension plasma sprayed hydroxyapatite coatings, *Journal of the European Ceramic Society* 37 (15) (2017) 5017 – 5021. doi:<https://doi.org/10.1016/j.jeurceramsoc.2017.07.007>. URL <http://www.sciencedirect.com/science/article/pii/S0955221917304831>
- [43] Y. Otsuka, Y. Hiraki, Y. Hakozaki, Y. Miyashita, Y. Mutoh, Effects of adhesive on reliability in interfacial strength evaluation method for plasma-sprayed hydroxyapatite coating, *Int. J. of Automation Technology* 11 (6) (2017) 907–904.
- [44] M. Shahien, M. Suzuki, Y. Tsutai, Controlling the coating microstructure on axial suspension plasma spray process, *Surface and Coatings Technology* 356 (2018) 96 – 107. doi:<https://doi.org/10.1016/j.surfcoat.2018.09.055>. URL <http://www.sciencedirect.com/science/article/pii/S0257897218310399>
- [45] R. T. Candidato, P. Sokołowski, L. Pawłowski, G. Lecomte-Nana, C. Constantinescu, A. Denoirjean, Development of hydroxyapatite coatings by solution precursor plasma spray process and their microstructural characterization, *Surface and Coatings Technology* 318 (2017) 39 – 49, 7th Rencontres Internationales de la Projection Thermique. doi:<https://doi.org/10.1016/j.surfcoat.2016.10.072>. URL <http://www.sciencedirect.com/science/article/pii/S0257897216310696>
- [46] B. Xu, D. Zhao, H. Y. Sohn, Y. Mohassab, B. Yang, Y. Lan, J. Yang, Flash synthesis of magneli' phase ($\text{TiO}_2\text{n}-1$) nanoparticles by thermal plasma treatment of H_2TiO_3 , *Ceramics International* 44 (4) (2018) 3929 – 3936. doi:<https://doi.org/10.1016/j.ceramint.2017.11.184>.

URL <http://www.sciencedirect.com/science/article/pii/S0272884217326548>

- [47] P. C. S.S. Scheerrer, M. Swain, Direct comparison of the bond strength result of the different test method:a critical literature review, *Dental Material* 26 (2) (2010) e78–e93.
- [48] R. Narayanan, S. Seshadri, T. Kwon, K. Kim, Calcium phosphate-based coatings on titanium and its alloys, *Journal of Biomedical Materials Research Part B: Applied Biomaterials: An Official Journal of The Society for Biomaterials, The Japanese Society for Biomaterials, and The Australian Society for Biomaterials and the Korean Society for Biomaterials* 85 (1) (2008) 279–299.
- [49] M. Bai, H. Maher, Z. Pala, T. Hussain, Microstructure and phase stability of suspension high velocity oxy-fuel sprayed yttria stabilised zirconia coatings from aqueous and ethanol based suspensions, *Journal of the European Ceramic Society* 38 (4) (2018) 1878 – 1887. doi:<https://doi.org/10.1016/j.jeurceramsoc.2017.10.026>.
URL <http://www.sciencedirect.com/science/article/pii/S0955221917307045>
- [50] A. C. M. Padilh, Charge storage oxygen deficient phases of tio₂: defect physics without defects, *Nature Material* 6 (28871).
- [51] W. Pompe, H. Worch, M. Epple, W. Friess, M. Gelinsky, P. Greil, U. Hempel, D. Scharnweber, K. Schulte, Functionally graded materials for biomedical applications, *Materials Science and Engineering: A* 362 (1) (2003) 40 – 60, papers from the German Priority Programme (Functionally Graded Materials). doi:[https://doi.org/10.1016/S0921-5093\(03\)00580-X](https://doi.org/10.1016/S0921-5093(03)00580-X).
URL <http://www.sciencedirect.com/science/article/pii/S092150930300580X>
- [52] H. Li, K. Khor, P. Cheang, Titanium dioxide reinforced hydroxyapatite coatings deposited by high velocity oxy-fuel (hvof) spray, *Biomaterials* 23 (1) (2002)

85–91. doi:10.1016/S0142-9612(01)00082-5.

URL <https://www.scopus.com/inward/record.uri?eid=2-s2.0-0036027447&doi=10.1016%2fS0142-9612%2801%2900082-5&partnerID=40&md5=f0c7f160a1ada9481d1fcb5183ac4ecd>

List of Figures

1	Experimental Procedure of Antibacterial Test	29
2	Microscopic Image of the Submicron Sized Powder Used as Feed-stock in SPS process (a) Hydroxyapatite powder (b) Ti_2O_3 Powder (c) Cumulative Size Distribution of the HAp Powder(blue) and Ti_2O_3 Powder(black) for Suspension Plasma Spray	30
3	Surface Features of SPS Coating on the Surface of Commercially Pure Titanium Material	30
4	Surface Morphology of the Coating Deposited by SPS technology at an optimized condition; (a), (b), (c) & (d) are the coating surface of 100H, 80H20T, 60H40T & 50H50T coating respectively. (e), (f), (g) & (h) are the corresponding higher magnification image.	31
5	Phase Identification of the Various Composition SPS Coating by XRD (a) 100H (b) 80H20T (c) 60H40T (d) 50H50T	32
6	Phase Identification of the Various Composition SPS Coating by Raman Spectroscopy (a) 100H (b) 80H20T (c) 60H40T (d) 50H50T	33
7	Quantitative Evaluation of Magneli Phase by Raman Peak fitting analysis and XRD Rietveld analysis Contained in Each Type of SPS coating	34
8	(a) Stress-Strain Curve and Corresponding AE Signal during Interfacial Strength Test for SPS coating. Detected AE Signal During Interfacial Strength Test (b) Typical AE Signal at Fracture (c) Corresponding FFT Signal. (d) Effect of composition on Interfacial Strength	34
9	Effect of Composition on Mechanical Properties of Suspension Plasma Sprayed HAp/ Titania Coating (a) Hardness (b) Young Modulus (c) Fracture Toughness	35
10	Wavelength Distribution Measured by Spectrometer of the Blue, Green, and Green Light; Used for Antibacterial Test.	35

11	Effect of Composition on Colony Forming Unit (CFU) Values of Suspension Plasma Sprayed HAp/ Titania Coating. Interaction effect of composition and laser irradiation was significant by two-way factorial ANOVA method. (Star symbol indicates that the value of p is less than 0.05)	36
12	(a) Quantitative histogram analysis of the density of live bacteria; Live/dead staining of E. coli cell on the surface of SPS coating (b) 100H (live cell) (c) 100H (dead cell) (d) 50H50T (live cell) (e) 50H50T (dead cell) . .	36
13	Wetability of the SPS coating was observed by measuring the contact angle of each type of coating	37
14	Comparing bacterial inhibition process during light irradiation between SPS and conventional composite coating	37

List of Tables

1	Optimized Operating condition of SPS method for fabrication of HAp composite coating	38
2	Thickness and Porosity Distribution of the Coating Deposited by SPS	38

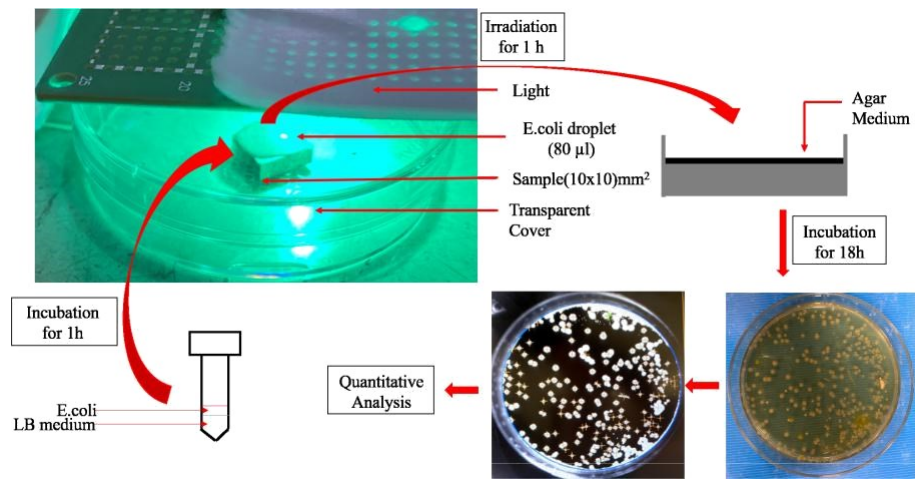


Figure 1: Experimental Procedure of Antibacterial Test

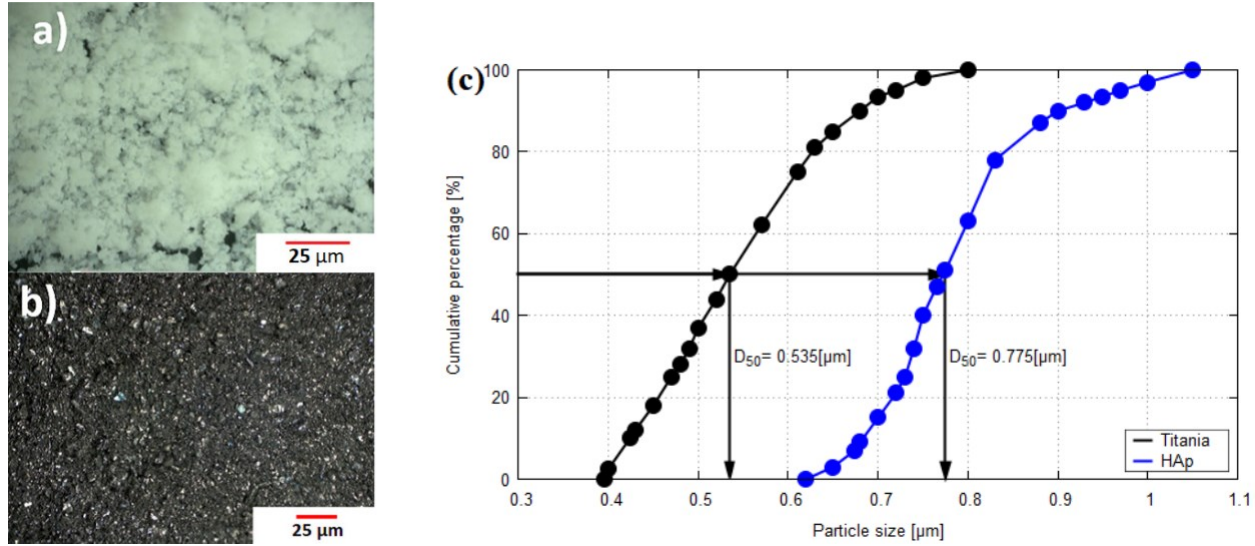


Figure 2: Microscopic Image of the Submicron Sized Powder Used as Feedstock in SPS process (a) Hydroxyapatite powder (b) Ti_2O_3 Powder (c) Cumulative Size Distribution of the HAp Powder (blue) and Ti_2O_3 Powder (black) for Suspension Plasma Spray

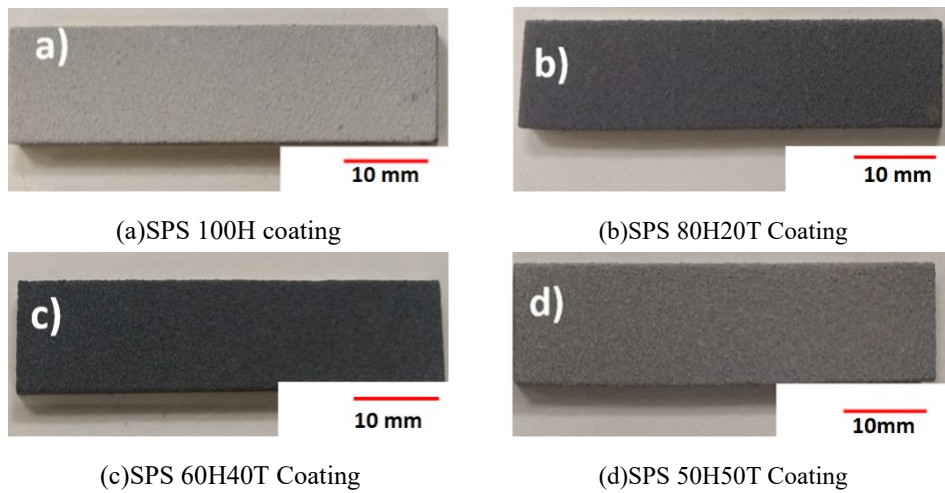


Figure 3: Surface Features of SPS Coating on the Surface of Commercially Pure Titanium Material

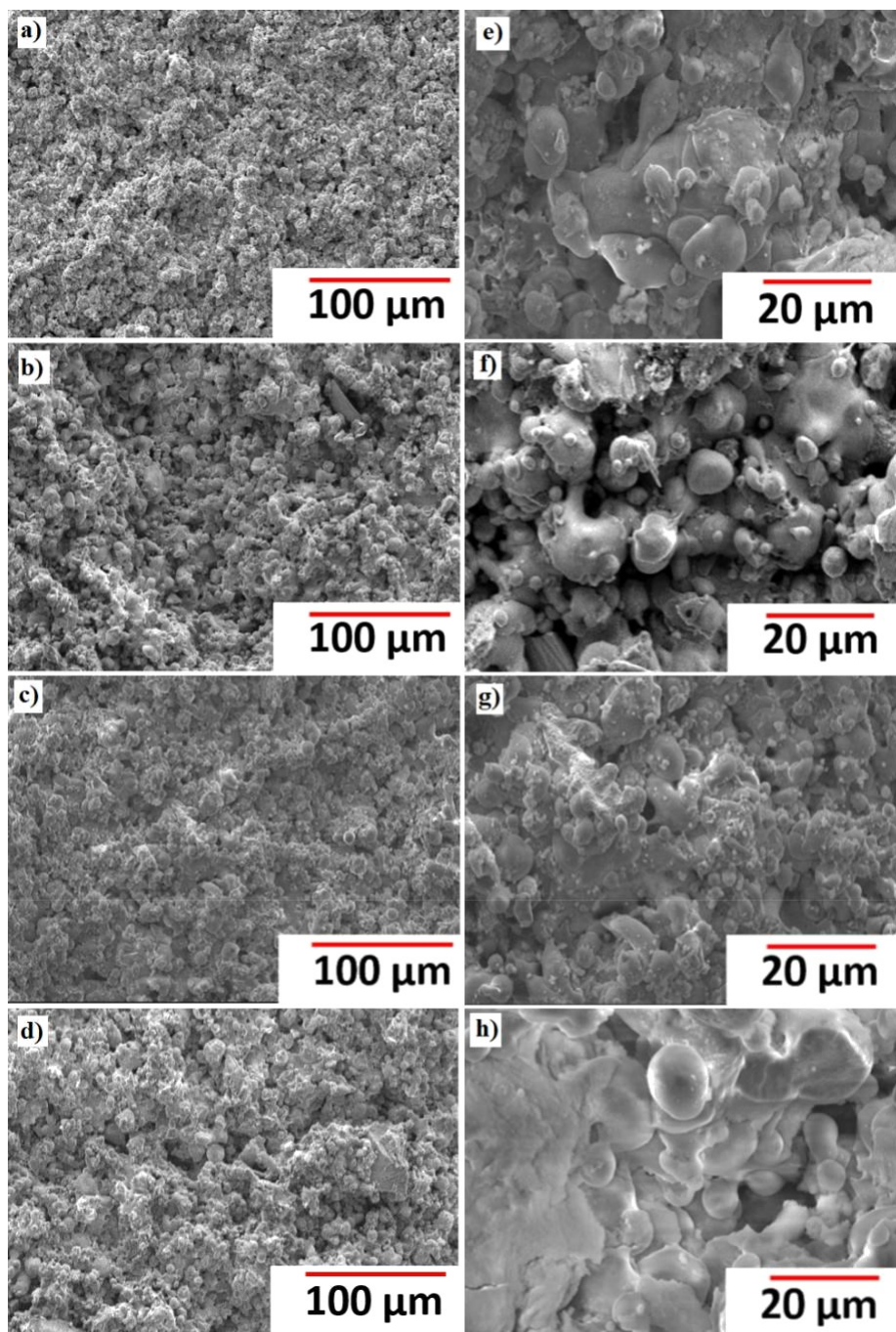


Figure 4: Surface Morphology of the Coating Deposited by SPS technology at an optimized condition; (a), (b), (c) & (d) are the coating surface of 100H, 80H20T, 60H40T & 50H50T coating respectively. (e), (f), (g) & (h) are the corresponding higher magnification image.

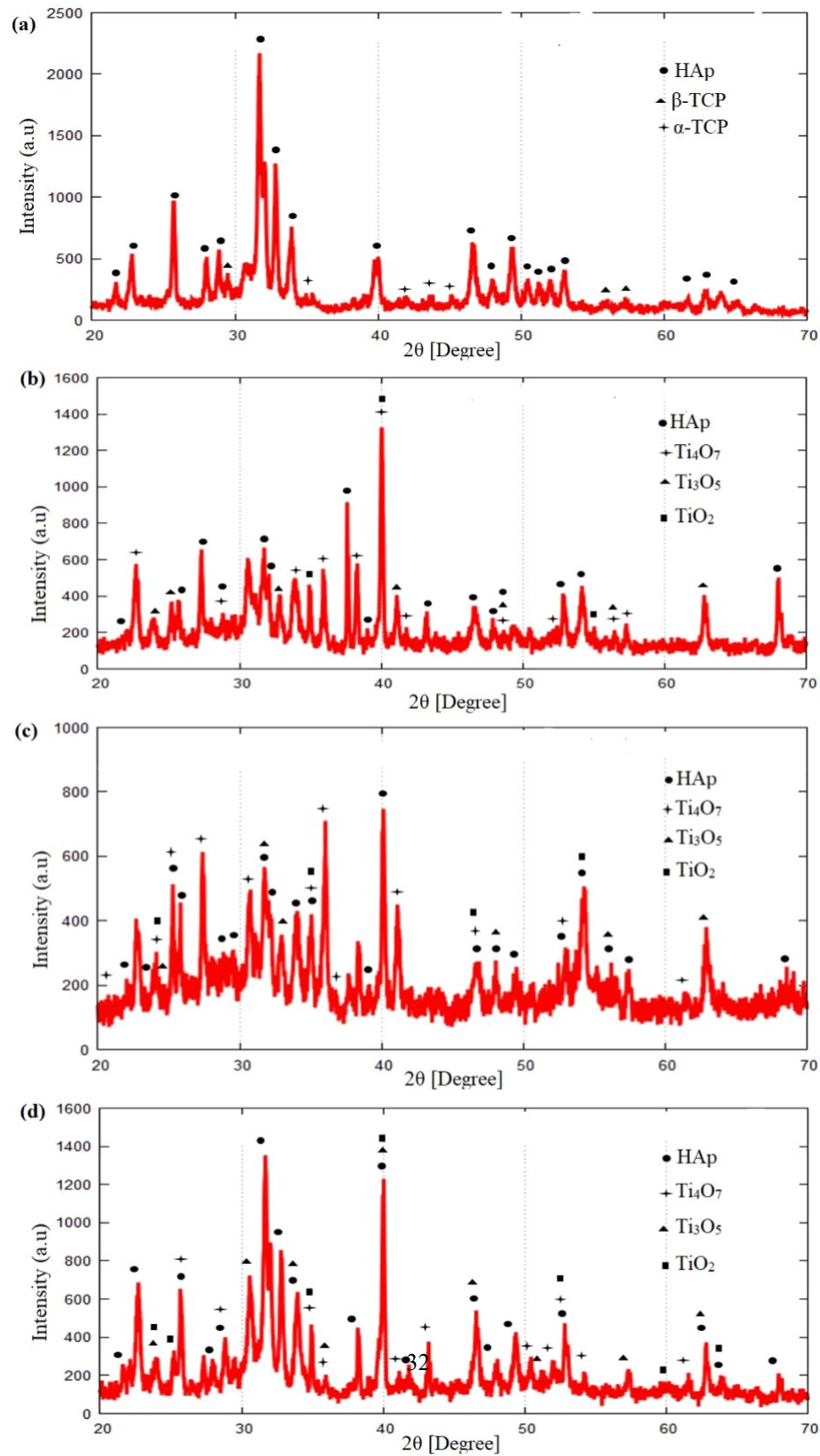


Figure 5: Phase Identification of the Various Composition SPS Coating by XRD (a) 100H (b) 80H20T (c)

60H40T (d) 50H50T

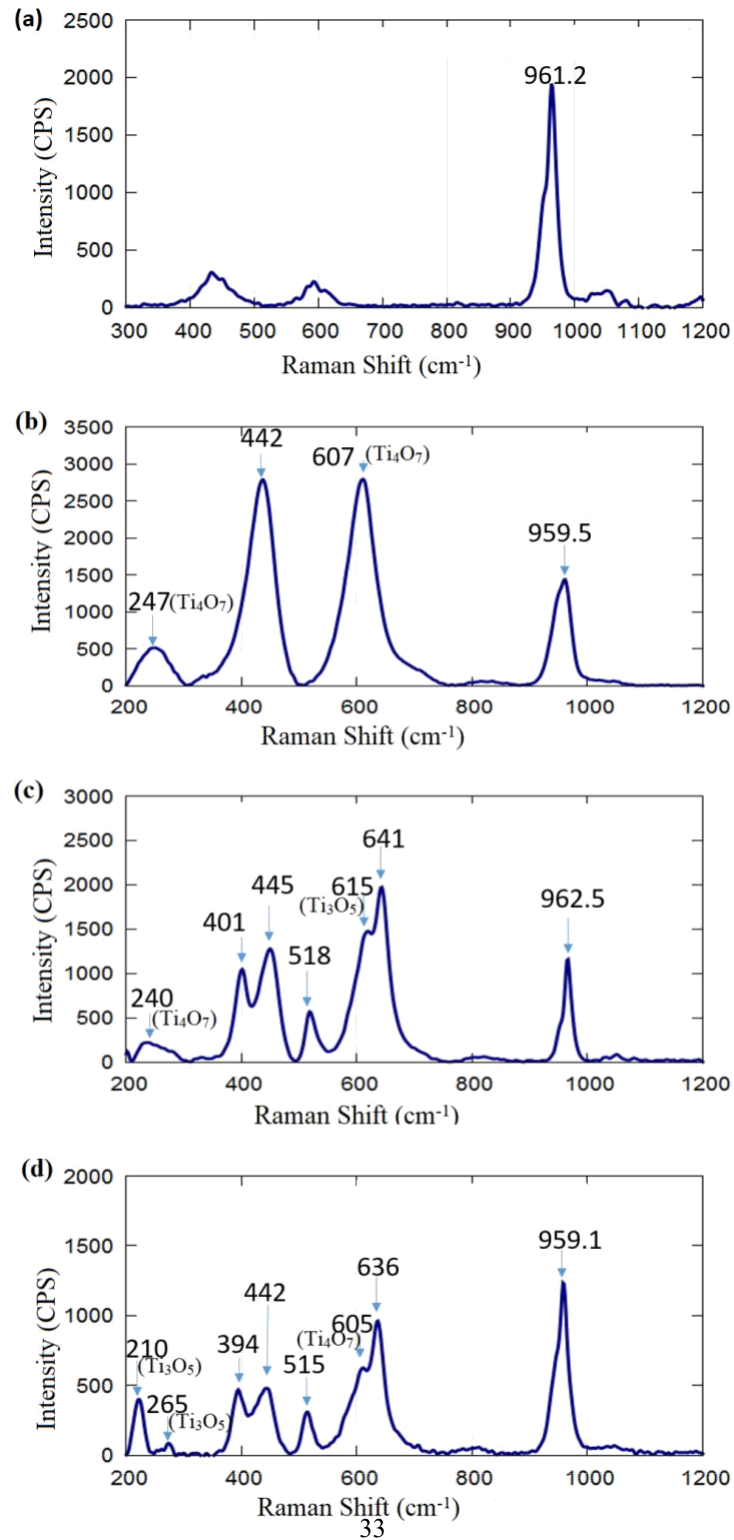


Figure 6: Phase Identification of the Various Composition SPS Coating by Raman Spectroscopy (a) 100H (b) 80H20T (c) 60H40T (d) 50H50T

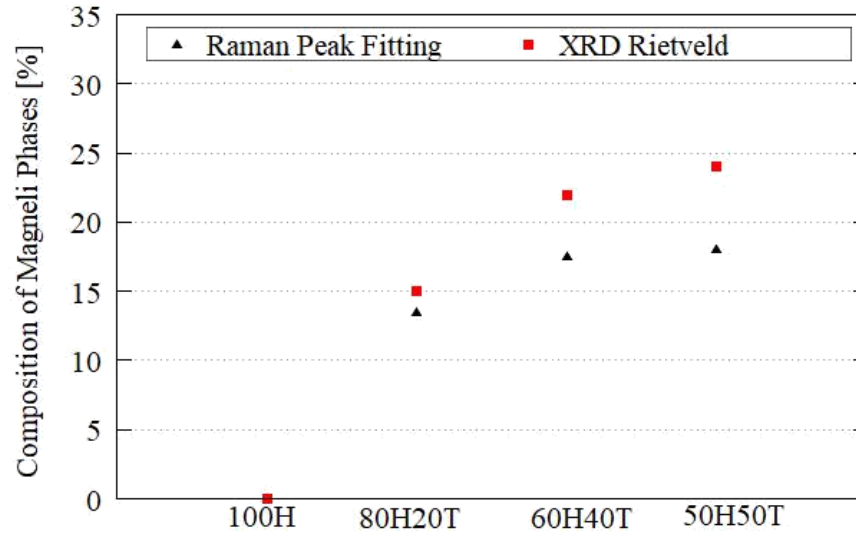


Figure 7: Quantitative Evaluation of Magneli Phase by Raman Peak fitting analysis and XRD Rietveld analysis Contained in Each Type of SPS coating

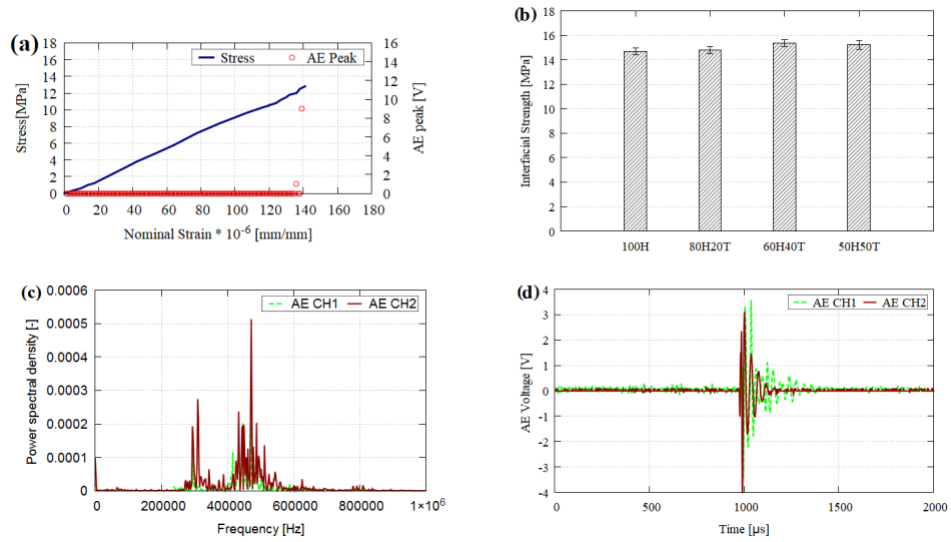


Figure 8: (a) Stress-Strain Curve and Corresponding AE Signal during Interfacial Strength Test for SPS coating. (b) Typical AE Signal at Fracture. (c) Corresponding FFT Signal. (d) Effect of composition on Interfacial Strength

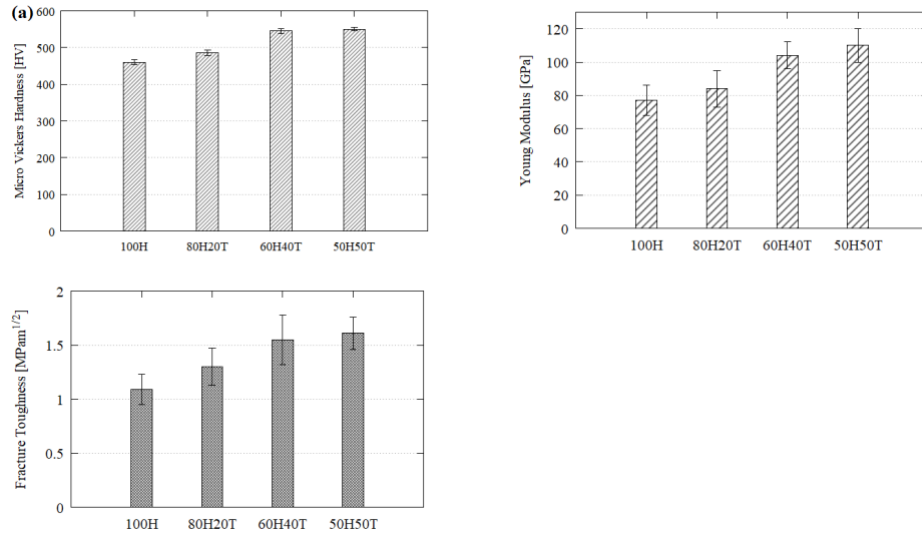


Figure 9: Effect of Composition on Mechanical Properties of Suspension Plasma Sprayed HAP/ Titania Coating (a) Hardness (b) Young Modulus (c) Fracture Toughness

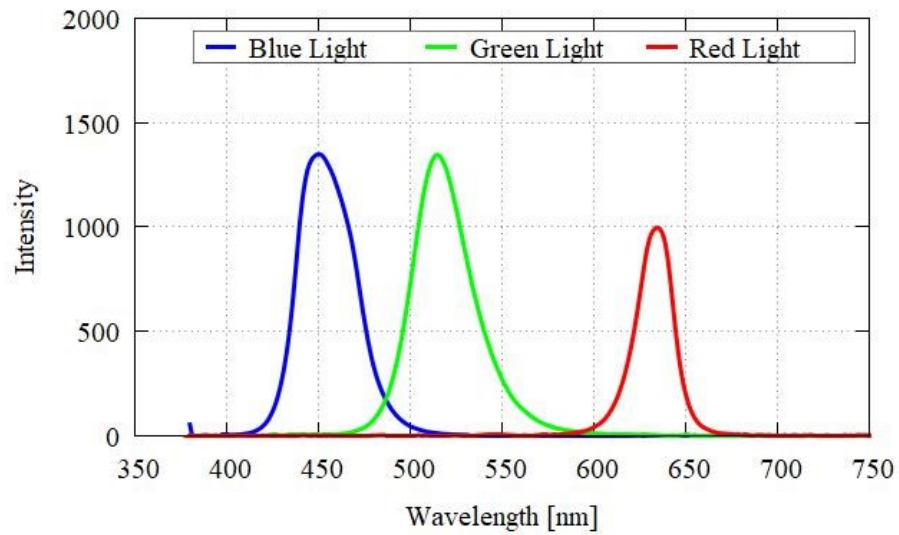


Figure 10: Wavelength Distribution Measured by Spectrometer of the Blue, Green, and Green Light; Used for Antibacterial Test

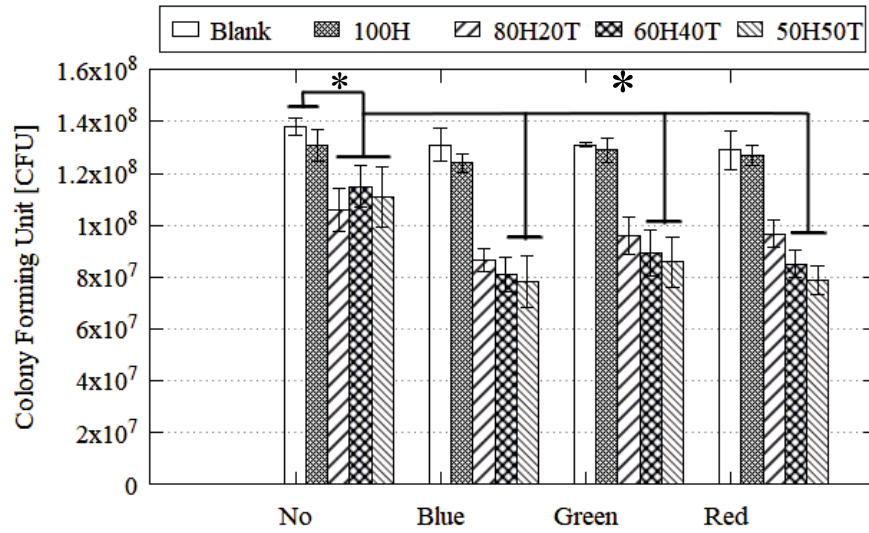


Figure 11: Effect of Composition on Colony Forming Unit (CFU) Values of Suspension Plasma Sprayed HAP/ Titania Coating. Interaction effect of composition and laser irradiation was significant by two-way factorial ANOVA method. (Star symbol indicates that the value of p is less than 0.05)

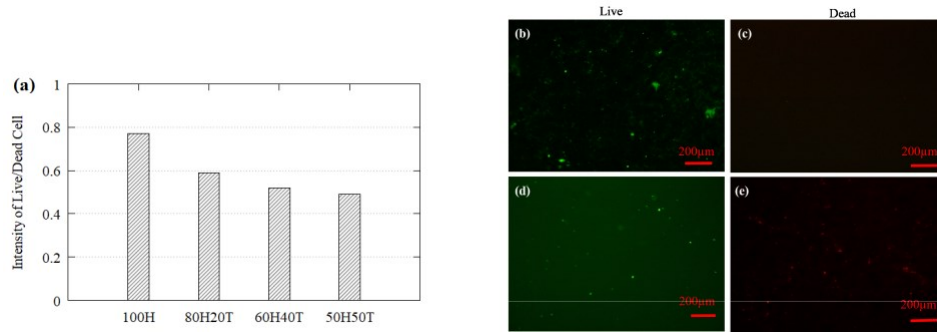


Figure 12: (a) Quantitative histogram analysis of the density of live bacteria; Live/dead staining of E. coli cell on the surface of SPS coating (b) 100H (live cell) (c) 100H (dead cell) (d) 50H50T (live cell) (e) 50H50T (dead cell)

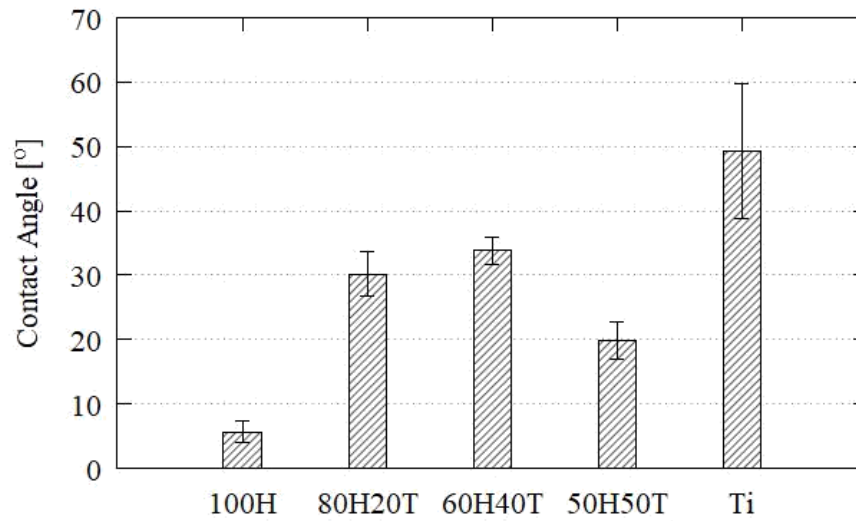


Figure 13: Wettability of the SPS coating was observed by measuring the contact angle of each type of coating

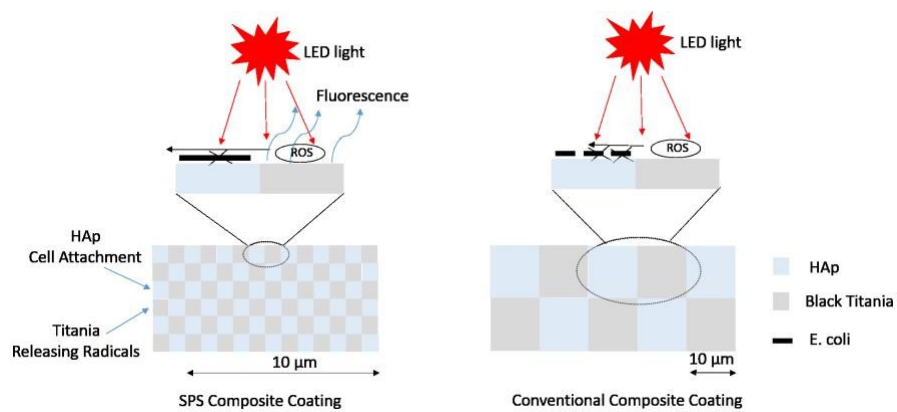


Figure 14: Comparing bacterial inhibition process during light irradiation between SPS and conventional composite coating

Table 1: Optimized Operating condition of SPS method for fabrication of HAp composite coating

Suspension Flow System		Plasma Spray	
Parameter	Value	Parameter	Value
Solvent Type	Water + Ethanol	Current(A)	600
Injection Pressure(MPa)	0.5	Voltage(V)	60
Nozzle ID(mm)	0.52	Spraying Distance (mm)	120
Flow Rate (ml/min)	55	Shield Gas	Ar
Solid Concentration (wt. %)	20,25	Coating Thickness (m)	100-150

Table 2: Thickness and Porosity Distribution of the Coating Deposited by SPS

Coating Type	Thickness (m)	Porosity (%)
SPS 100H	75 10	11.4 2.9
SPS 80H20T	90 22	10.3 1.9
SPS 60H40T	105 25	7.5 2.1
SPS 50H50T	100 20	8.1 3.1